

Article

Preparation of (GaZn)(NO) Photocatalysts from the Reaction of NH with GaO/ZnO and ZnGaO: In Situ Time-Resolved XRD and XAFS Studies

Haiyan Chen, Wen Wen, Qi Wang, Jonathan C. Hanson, James T. Muckerman, Etsuko Fujita, Anatoly I. Frenkel, and Jose# A. Rodriguez

J. Phys. Chem. C, **2009**, 113 (9), 3650-3659 • DOI: 10.1021/jp804551p • Publication Date (Web): 05 February 2009

Downloaded from <http://pubs.acs.org> on February 28, 2009

More About This Article

Additional resources and features associated with this article are available within the HTML version:

- Supporting Information
- Access to high resolution figures
- Links to articles and content related to this article
- Copyright permission to reproduce figures and/or text from this article

[View the Full Text HTML](#)

Preparation of $(\text{Ga}_{1-x}\text{Zn}_x)(\text{N}_{1-x}\text{O}_x)$ Photocatalysts from the Reaction of NH_3 with $\text{Ga}_2\text{O}_3/\text{ZnO}$ and ZnGa_2O_4 : In Situ Time-Resolved XRD and XAFS Studies

Haiyan Chen,[†] Wen Wen,[†] Qi Wang,[§] Jonathan C. Hanson,[†] James T. Muckerman,^{†,‡} Etsuko Fujita,[†] Anatoly I. Frenkel,[§] and José A. Rodríguez^{*,†}

Chemistry Department, Brookhaven National Laboratory, Upton, New York 11973, Center for Functional Nanomaterials, Brookhaven National Laboratory, Upton, New York 11973, and Department of Physics, Yeshiva University, 245 Lexington Avenue, New York, New York 10016

Received: May 22, 2008; Revised Manuscript Received: November 19, 2008

Gallium zinc oxynitrides $(\text{Ga}_{1-x}\text{Zn}_x)(\text{N}_{1-x}\text{O}_x)$ are important due to their visible-light photocatalytic activity. Using in situ time-resolved X-ray diffraction (XRD), we have monitored the formation of wurtzite $(\text{Ga}_{1-x}\text{Zn}_x)(\text{N}_{1-x}\text{O}_x)$ compounds during the solid-state reaction of NH_3 with $\text{Ga}_2\text{O}_3/\text{ZnO}$ mixtures or a ZnGa_2O_4 spinel. The ZnGa_2O_4 spinel was found to be a key intermediate in the formation of $(\text{Ga}_{1-x}\text{Zn}_x)(\text{N}_{1-x}\text{O}_x)$ and imposes a limit on the zinc content in the gallium zinc oxynitrides. Furthermore, after its formation, a wurtzite $(\text{Ga}_{2/3}\text{Zn}_{1/3})(\text{N}_{2/3}\text{O}_{1/3})$ phase evolves to $(\text{Ga}_{0.9}\text{Zn}_{0.1})(\text{N}_{0.9}\text{O}_{0.1})$ with increasing nitridation reaction time as a result of the removal of Zn and O atoms from the system. Once $(\text{Ga}_{2/3}\text{Zn}_{1/3})(\text{N}_{2/3}\text{O}_{1/3})$ is formed, one must minimize exposure of the compound to NH_3 . Zinc and gallium K-edge X-ray absorption fine structure (XAFS) data revealed that the local structures around gallium and zinc atoms in the $(\text{Ga}_{1-x}\text{Zn}_x)(\text{N}_{1-x}\text{O}_x)$ systems are similar to those of GaN and ZnO, respectively, with relatively minor distortions in the Ga–N and Zn–O bond lengths. The Zn–O/N bonds prefer to align along the *c*-axis of the lattice, in agreement with the findings of DFT calculations reported in the literature. The corresponding Zn K-edge XANES spectra of $(\text{Ga}_{1-x}\text{Zn}_x)(\text{N}_{1-x}\text{O}_x)$ display a position red-shifted toward lower energies by ~ 0.5 eV with respect to that of ZnO, indicating a lower oxidation state of Zn in $(\text{Ga}_{1-x}\text{Zn}_x)(\text{N}_{1-x}\text{O}_x)$. N K-edge NEXAFS data show that the bonding geometry and electronic properties of the nitrogen atoms in $(\text{Ga}_{1-x}\text{Zn}_x)(\text{N}_{1-x}\text{O}_x)$ are similar to those in GaN. However, the O K-edge spectra exhibit a pre-edge feature not seen for ZnO or Ga_2O_3 . This unique property of the oxygen atoms in $(\text{Ga}_{1-x}\text{Zn}_x)(\text{N}_{1-x}\text{O}_x)$ may be related to the existence of holes and affect visible light absorption and surface chemistry.

I. Introduction

The strong scientific and technological drive to utilize solar energy to generate clean hydrogen fuel from the photocatalytic splitting of water¹ has drawn intensive research effort to the investigation of anion doped metal oxide catalysts, especially nitrogen-doped metal oxide photocatalysts. Among the tested visible-light-active photocatalyst candidates, cocatalyst-loaded $(\text{Ga}_{1-x}\text{Zn}_x)(\text{N}_{1-x}\text{O}_x)$ boasts a quantum efficiency of 2–3% for water splitting at wavelengths between 420 and 440 nm.^{2–4} Experimentally, the synthesis of this type of photocatalyst is accomplished by heating a mixture of Ga_2O_3 and ZnO in ammonia at high temperatures (> 800 °C).^{2–12} The microscopic understanding of this synthesis process is quite limited. In situ studies are necessary to establish the mechanism for $(\text{Ga}_{1-x}\text{Zn}_x)(\text{N}_{1-x}\text{O}_x)$ formation. For example, various experimental attempts, including using excess amounts of ZnO and shorter annealing times, have been made to increase the zinc content in the photocatalyst. However, until now, the Zn/(Ga + Zn) ratio obtained from the nitridation reaction is typically below 1/3. As a solid solution, $(\text{Ga}_{1-x}\text{Zn}_x)(\text{N}_{1-x}\text{O}_x)$ is composed of GaN and ZnO, two materials with the same hexagonal

wurtzite structure and closely matched lattice constants.^{2,4,13} Therefore, $(\text{Ga}_{1-x}\text{Zn}_x)(\text{N}_{1-x}\text{O}_x)$ systems with a Zn/(Ga + Zn) ratio larger than 1/3 should be stable and accessible by synthesis. Indeed, this idea is supported by the results of recent density-functional calculations.¹³ Furthermore, the theoretical calculations have shown that $(\text{Ga}_{1-x}\text{Zn}_x)(\text{N}_{1-x}\text{O}_x)$ compounds with a Zn/(Ga + Zn) ratio around 0.5 could be very efficient photocatalysts for the splitting of water with solar energy.¹³ To prepare more efficient catalysts demands the development of new synthesis strategies based on a thorough understanding of the solid-state reaction mechanism.

Investigations into the structural and electronic properties of $(\text{Ga}_{1-x}\text{Zn}_x)(\text{N}_{1-x}\text{O}_x)$ photocatalysts are essential for understanding the interplay of structure–activity relationships. $(\text{Ga}_{1-x}\text{Zn}_x)(\text{N}_{1-x}\text{O}_x)$ is a complicated quaternary system in which the Ga and Zn atoms or the N and O atoms are inconveniently close in atomic properties. This system presents great challenges to various characterization techniques in terms of distinguishing Ga from Zn and N from O. To date, neutron and X-ray diffraction (XRD) characterizations have been applied to probe the long-range order of these photocatalysts.^{14,15} It was found that these photocatalysts are single-phased hexagonal wurtzite solid solutions without interstitial or large disorder in terms of oxygen and nitrogen.¹⁴ However, a recent report pointed out that the visible light absorption of $(\text{Ga}_{1-x}\text{Zn}_x)(\text{N}_{1-x}\text{O}_x)$ originates from Zn or O related impurity states, which could be taken as a sign of the presence of distortions or other lattice defects.¹⁶

* Author to whom correspondence should be addressed at the Chemistry Department, Brookhaven National Laboratory, Upton, NY 11973. Telephone: (+1) 631-344-2246. Fax: (+1) 631-344-5815. E-mail: rodriguez@bnl.gov.

[†] Chemistry Department, Brookhaven National Laboratory.

[‡] Center for Functional Nanomaterials, Brookhaven National Laboratory.

[§] Department of Physics, Yeshiva University.

Neutron and XRD diffraction can only produce information on long-range order,^{14,15,17} and in the particular case of (Ga_{1-x}Zn_x)(N_{1-x}O_x), without distinction between Ga and Zn. Probing the bulk and surface local bonding and short-range order with X-ray absorption fine structure (XAFS) should allow us to detect disorders to which XRD is blind.¹⁸

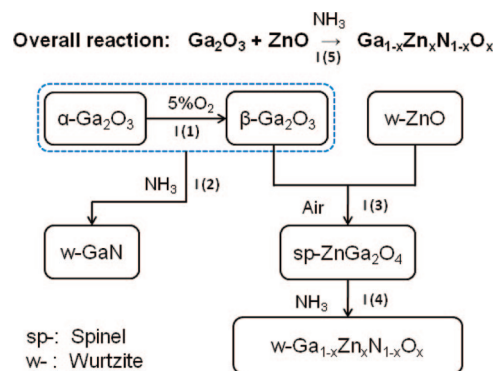
In this article, we will use a combination of in situ time-resolved XRD and XAFS to study the synthesis plus the structural and electronic properties of (Ga_{1-x}Zn_x)(N_{1-x}O_x) compounds. In the exploration of the reaction mechanism, in situ time-resolved XRD is a very powerful tool for the identification of possible reaction intermediates and the study of phase transformations.¹⁷ This technique has shed light on several interesting puzzles in heterogeneous catalysis.¹⁷ XAFS is sensitive to local structures of specific absorbing atoms.¹⁸ X-ray absorption near edge structure (XANES) and extended X-ray absorption fine structure (EXAFS) were used to explore the local atomic structure, short-range order, and electronic properties of (Ga_{1-x}Zn_x)(N_{1-x}O_x). The article is organized as follows. Section II describes the details of the experimental set up utilized for the XRD and XAFS measurements. In section III.1, we examine structural details associated with the preparation of gallium zinc oxynitrides through the reaction of Ga₂O₃/ZnO or ZnGa₂O₄ with ammonia. Sections III.2 and III.3 are devoted to study the structural and electronic properties of the synthesized (Ga_{1-x}Zn_x)(N_{1-x}O_x) photocatalysts.

II. Experimental Section

For ex situ XRD, NEXAFS, XANES, and EXAFS characterizations, the samples were made by thermal annealing of mixtures of Ga₂O₃ (Alfa-Aesar, 99.99%) and ZnO (Alfa-Aesar, 99.99%) powders under a pure NH₃ (Praxair, 99.999%) flow in a quartz tube reactor heated by a temperature programmed tubular furnace.¹⁹ For in situ XRD experiments, the mixtures of Ga₂O₃ and ZnO with different molar ratio were loaded into a sapphire capillary (inner diameter 0.7 mm) cell specifically designed for time-resolved in situ XRD monitoring.^{20,21} A mixture of 5% of NH₃ in helium (Praxair) was admitted into the cell at a flow rate of ~10 mL/min through the flow system. The capillary was heated by a resistive heater wrapped around the capillary at the temperature ramp rate of ~2 °C/min. The temperature was monitored with a 0.5-mm type K thermocouple inside the capillary and was program controlled using a temperature controller. The time-resolved X-ray diffraction experiments were carried out on beamline X7B (λ = 0.922 Å) of the National Synchrotron Light Source (NSLS) at Brookhaven National Laboratory. Unless otherwise specified, the flow rate of the gas mixture, the temperature ramp rate, and the X-ray wavelength, were as indicated above for all in situ XRD experiments. In situ diffraction patterns were collected during nitridation at ~4-min intervals with a MAR345 image plate detector. XRD patterns were analyzed using the software GSAS (General Structure Analysis System code developed by A. C. Larson and R. B. Von Dreele at Los Alamos National Laboratory, Report LAUR 86-784, 2004) interfaced with EXPGUI²² and the Reflex module of Materials Studio (Accelrys).

Nitrogen and oxygen K-edge NEXAFS spectra were taken at the NIST/DOW end station at beamline U7A of the NSLS.²³ The PEY signal was collected using a Channeltron electron multiplier with an adjustable entrance grid bias (EGB) of -150 V. A low-energy electron flood gun was used to compensate for charging effects. Gallium and zinc K-edge XANES and EXAFS data were collected at beamlines X18B and X19A of

SCHEME 1: In Situ XRD studies Performed and Presented in this Paper^a

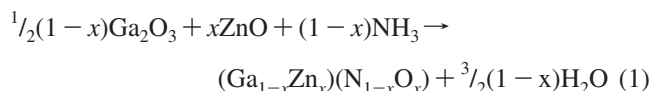


^a Each arrow in the scheme represents an in situ XRD investigation that is discussed in sections III.1.I(1) to III.1.I(5) as indicated by a section number next to the arrow.

the NSLS using either the transmission or fluorescence detection mode, and the data were processed using the Athena and Artemis software packages.²⁴

III. Results and Discussions

III.1. Reaction Mechanism and Phase Transformations in the Synthesis of (Ga_{1-x}Zn_x)(N_{1-x}O_x): In situ time-resolved XRD studies. The synthesis of wurtzite (Ga_{1-x}Zn_x)(N_{1-x}O_x) from structurally different Ga₂O₃ and another wurtzite species ZnO in a gas solid reaction process involves multiple phase transitions as a result of temperature changes and/or chemical reactions. The overall synthesis reaction can be expressed as:



As we will see, this process includes the intermediate formation of spinel ZnGa₂O₄. The following reaction steps or competing reactions were studied and will be described below: (1) thermal transformation of α- to β-Ga₂O₃, (2) the formation of GaN from β-Ga₂O₃ and NH₃, (3) the formation of spinel ZnGa₂O₄ from ZnO and β-Ga₂O₃ in air, (4) the formation of (Ga_{1-x}Zn_x)(N_{1-x}O_x) from spinel ZnGa₂O₄ and NH₃, and (5) the overall reaction of ZnO/Ga₂O₃ with NH₃. The relevance of each reaction step to the overall reaction is illustrated in Scheme 1.

III.1.I(1) α-Ga₂O₃ to β-Ga₂O₃ Transition. The commercial Ga₂O₃ powder, one of the starting oxides, is a mixture of rhombohedral α-Ga₂O₃ and monoclinic β-Ga₂O₃ polymorphs. Upon annealing in 5% O₂ in helium, the α phase is converted to the high-temperature-stable β phase without any observable intermediates (See Figure 1). Under our experimental conditions, the transition is completed around 630 °C. The conversion of α-Ga₂O₃ to β-Ga₂O₃ was reported to occur between 500 and 750 °C in an ex situ measurement.²⁵ In the flow of 5% NH₃ in helium, the thermal transformation took place around ~780 °C. As illustrated in Figure M1 of Supporting Information, the β phase contains a mixture of 4- and 6-coordinated Ga atoms while the α phase contains only 6-coordinated Ga atoms. During the α to β phase transition, some of the Ga atoms become 4-coordinated. This 6- to 4-coordinated Ga transformation is important because in the final product of (Ga_{1-x}Zn_x)(N_{1-x}O_x) Ga atoms are 4-coordinated.

III.1.I(2) Reaction of NH₃ with Ga₂O₃. The in situ XRD patterns during the reaction of Ga₂O₃ with ammonia are shown in Figure 2. From these patterns, the α-Ga₂O₃ to β-Ga₂O₃ phase

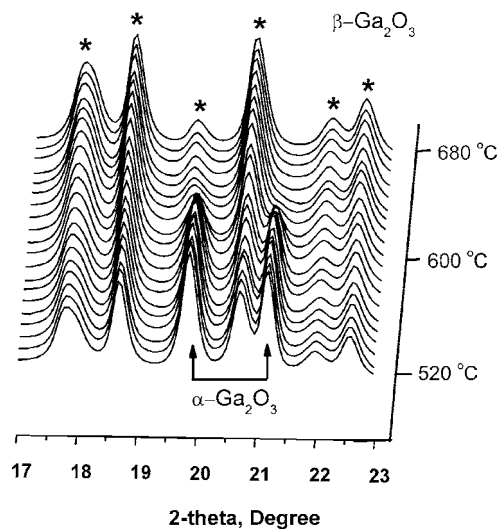


Figure 1. In situ XRD patterns of the phase transition from α -Ga₂O₃ to β -Ga₂O₃ during annealing of commercial Ga₂O₃ in 5% O₂ in helium. The peak positions of β -Ga₂O₃ are indicated by the “*” symbols.

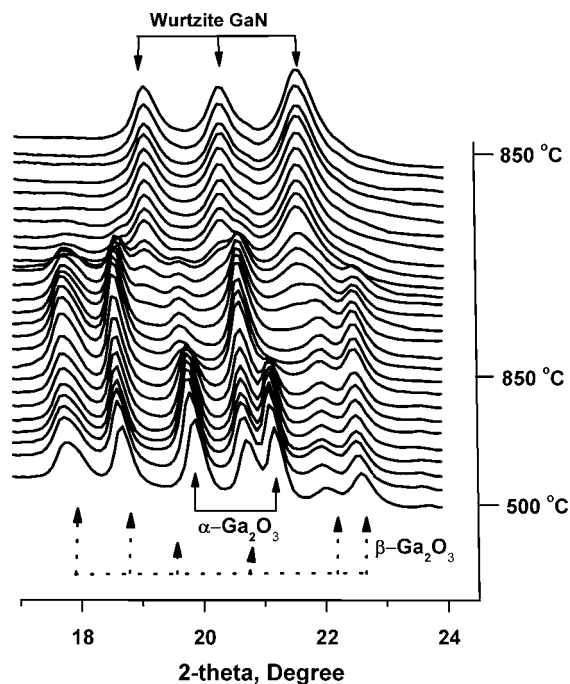


Figure 2. In situ XRD patterns during the annealing of commercial Ga₂O₃ in 5% ammonia in helium.

transition was observed and the complete conversion takes place around 780 °C. The transition between β -Ga₂O₃ and GaN took place relatively rapidly after an induction period of 5 h. During the transformation, the β phase was found to coexist with GaN as demonstrated by the XRD patterns. There is no completely amorphous pattern in the series of patterns. This rules out the postulated completely amorphous intermediate phase.^{26,27} However, we could not detect if the amorphous phases coexisted with β -Ga₂O₃ and GaN. In an ammonia atmosphere, therefore, the most likely scenario is the conversion of α -Ga₂O₃ to β -Ga₂O₃ to generate 4-coordinated Ga atoms and then β -Ga₂O₃ to wurtzite GaN.

III.1.1(3) Formation of Spinel ZnGa₂O₄ from ZnO and β -Ga₂O₃. The batch synthesis of ZnGa₂O₄ from ZnO and Ga₂O₃ is known.²⁸ We performed an in situ XRD-monitored synthesis of spinel ZnGa₂O₄ from annealing wurtzite ZnO and β -Ga₂O₃ in air (see Figure 3). The phase that emerged at \sim 700 °C was

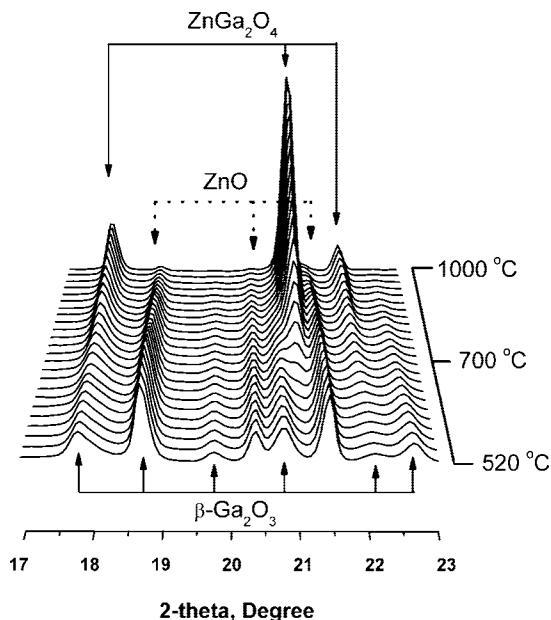


Figure 3. In situ XRD monitored synthesis of spinel ZnGa₂O₄ from annealing β -Ga₂O₃ and ZnO in air under ambient pressure. The temperature ramp rate is \sim 3 °C/min.

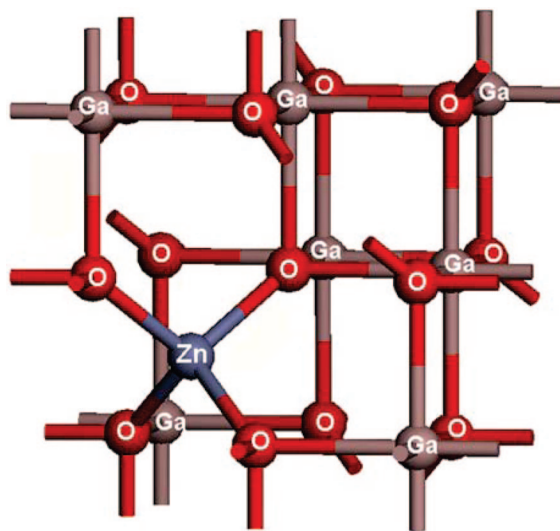


Figure 4. Ball-and-stick model of $1/8$ of the unit cell for the cubic spinel ZnGa₂O₄.

attributed to spinel ZnGa₂O₄. The lattice constant of the product was determined to be 8.331(1) Å and in agreement with the literature value of 8.331 Å for ZnGa₂O₄ (JCPDS Card no. 38-1249). The formation of spinel ZnGa₂O₄ allows the Zn atoms and Ga atoms to be incorporated in the same lattice. The coexistence of Zn and Ga in the spinel is the structural foundation for the coexistence of these two types of atoms in the (Ga_{1-x}Zn_x)(N_{1-x}O_x) final products.

III.1.1(4) Formation of (Ga_{1-x}Zn_x)(N_{1-x}O_x) from Spinel ZnGa₂O₄ and NH₃. Before describing the conversion of spinel ZnGa₂O₄ to wurtzite (Ga_{1-x}Zn_x)(N_{1-x}O_x), an examination of the crystal structure of ZnGa₂O₄ is helpful for visualizing the reaction mechanisms. In the spinel ZnGa₂O₄ lattice, shown in Figure 4, the Zn atoms are in tetrahedral sites and the Ga atoms are in octahedral sites. The bond length of Zn–O and Ga–O is 1.900 and 2.027 Å, respectively, with the bond length of Ga–O longer than Ga–N in GaN and the bond length of Zn–O shorter than that in ZnO. In wurtzite GaN and ZnO, Ga and Zn atoms

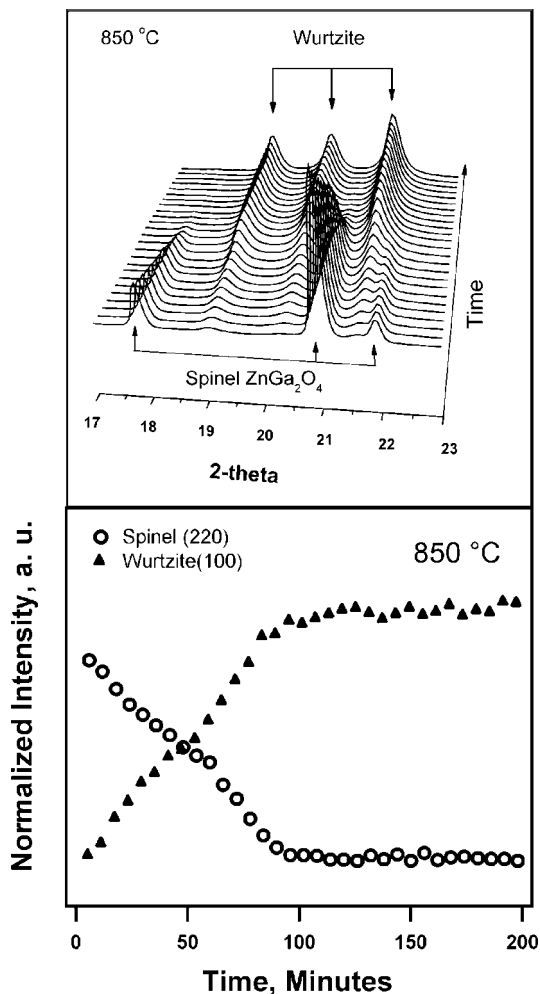


Figure 5. Phase transition from spinel ZnGa_2O_4 to wurtzite $(\text{Ga}_{1-x}\text{Zn}_x)(\text{N}_{1-x}\text{O}_x)$. Presented in the upper panel are the in situ XRD patterns during annealing of ZnGa_2O_4 in 5% ammonia in helium at 850°C . The lower panel displays the intensity changes of spinel ZnGa_2O_4 and wurtzite with time.

occupy tetrahedral sites. Therefore, in the spinel to wurtzite phase transition, since the Zn atoms are already at tetrahedral sites, they do not have to go through a dramatic geometric reconfiguration. However, the Zn–O bond length in ZnGa_2O_4 is shorter than that in ZnO and needs to be elongated. For transforming the Ga atoms at octahedral sites in the spinel ZnGa_2O_4 to tetrahedral sites in wurtzite $(\text{Ga}_{1-x}\text{Zn}_x)(\text{N}_{1-x}\text{O}_x)$, at least two Ga–O bonds have to be broken and the associated oxygen atoms removed. Some or all of the four oxygen atoms in the remaining Ga–O bonds should be replaced by nitrogen atoms. From the point view of bond enthalpy, the Zn–O bond is weaker (1.65 eV) than the Ga–O bond (3.66 eV)²⁹ and is easier to break. This suggests that Ga–O bond breaking could be the rate-limiting step in this phase transition.

The conversion of spinel ZnGa_2O_4 to wurtzite $(\text{Ga}_{1-x}\text{Zn}_x)(\text{N}_{1-x}\text{O}_x)$ was accomplished by isothermal heating in ammonia at 850 and 900°C . From the in situ XRD patterns of this reaction at 850°C shown in the upper panel of Figure 5, this phase transition does not involve any intermediate phase. Shown in the lower panel of Figure 5, the linear decrease of the spinel phase with time at the initial stage is mirrored by the increase of the wurtzite phase. The linear decrease of the spinel phase with time indicates a zeroth-order reaction of a surface or interface nature. Following the same methodology described in previous studies,^{30,31} an apparent activation energy of 3.7 ± 0.3

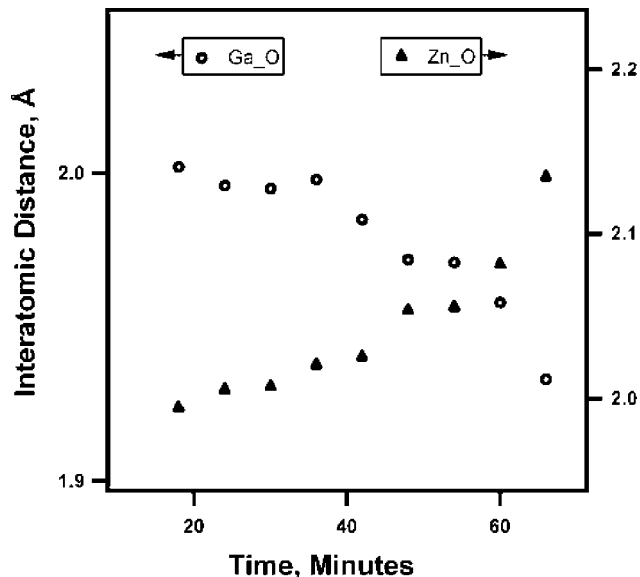


Figure 6. The change in interatomic distances of Ga–O and Zn–O in spinel ZnGa_2O_4 as a function of time during annealing of ZnGa_2O_4 in 5% NH_3 in helium at 850°C . The distances are obtained from X-ray profile refinement (GSAS) and the standard deviations for Ga–O and Zn–O interatomic distances are less than 0.01 and 0.03 Å, respectively.

eV was obtained. In a first approximation, due to the narrow temperature window, two data points at 850 and 900°C were used to estimate the activation energy by the Arrhenius equation. The integrated peak intensity for the spinel (311) line is proportional to the fraction of ZnGa_2O_4 in the sample.^{30,31} Using a least-squares fitting of the slope for the decrease of the normalized integrate intensity of the spinel (311) peak versus time, the reaction rate constant was determined to be $-(0.0111 \pm 0.0004) \text{ min}^{-1}$ at 850°C , and $-(0.018 \pm 0.001) \text{ min}^{-1}$ at 900°C . These values could be refined in the future by performing in situ measurements of neutron diffraction or a pair distribution function (PDF) analysis.³² In any case, the estimated apparent activation energy is much closer to a value of 3.66 eV, the bond enthalpy of Ga–O, than to a value of 1.65 eV, the bond enthalpy of Zn–O.²⁹ This implies that Ga–O bond breaking may be the rate-limiting step in the formation of $(\text{Ga}_{1-x}\text{Zn}_x)(\text{N}_{1-x}\text{O}_x)$ from the reaction of ZnGa_2O_4 with ammonia. DFT calculations performed in our Laboratory also support this idea.

A plot of bond distances based on Rietveld analysis of the in situ XRD patterns displayed in Figure 5 showed the elongation of the Zn–O bond (see Figure 6). With the progress of nitridation at 850°C , the Zn–O interatomic distance increases from 1.994(14) to 2.134(26) Å. The Ga–O interatomic distance, at the same time, decreases from 2.002(7) to 1.933(12) Å. At room temperature, the bond length of Zn–O in ZnGa_2O_4 is 1.900 Å, shorter than those in ZnO (1.996 Å along *c*-axis and 1.968 Å in other directions). The bond length of Ga–O, on the other hand, is 2.027 Å, longer than those in GaN (1.955 Å along *c*-axis and 1.946 Å along other directions). In the reaction of ZnGa_2O_4 with NH_3 , the elongation of Zn–O bonds and compression of the Ga–O bonds brings the interatomic distances into the range they exhibit in ZnO and GaN. The lengthening of the Zn–O bond could eventually lead to the break of the Zn–O bond and may be related to the depletion of Zn from the spinel ZnGa_2O_4 .

III.1.1(5) Reaction of NH_3 with $\text{Ga}_2\text{O}_3/\text{ZnO}$. The in situ XRD patterns of the overall reaction (1) are displayed in Figure 7. The main events related to phase transitions which have been discussed in previous sections are:

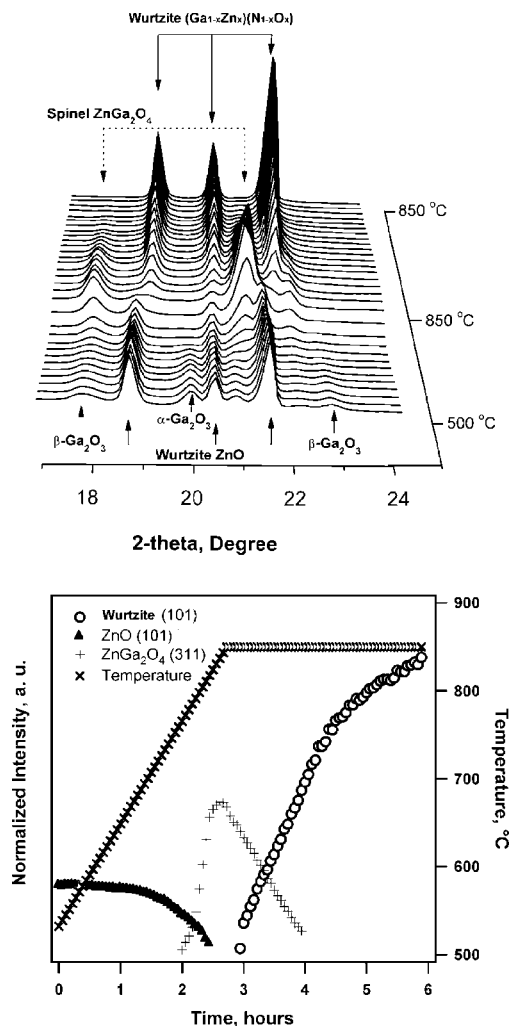
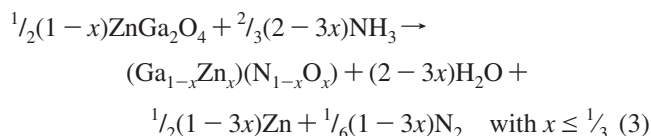


Figure 7. Upper panel: in situ XRD patterns during the annealing of a mixture of commercial Ga₂O₃/ZnO in 5% NH₃ in helium. The mixture of Ga₂O₃ and ZnO with a molar ratio of Zn/Ga = 1:1 was used in this study, and the temperature profile of this nitridation reaction is displayed in the lower panel. Lower panel: the variation of the XRD peak intensity of ZnO(101), spinel ZnGa₂O₄(311) and wurtzite(101) with nitridation time and temperature. The intensities are extracted from the in situ XRD patterns shown in the upper panel and are normalized to the beam current.

1. The transition from α -Ga₂O₃ to β -Ga₂O₃.
2. The transition from β -Ga₂O₃ and wurtzite ZnO to spinel ZnGa₂O₄:



3. The transition from spinel ZnGa₂O₄ to wurtzite (Ga_{1-x}Zn_x)(N_{1-x}O_x):



In Figure 7, showing the XRD patterns of the starting metal oxides, the intense peaks from wurtzite ZnO masked several peaks related to Ga₂O₃. As a result, compared to Figure 1, only one peak related to rhombohedral α -Ga₂O₃ and two peaks related to monoclinic β -Ga₂O₃ could be clearly seen. Similar to the thermal transformation reaction of Ga₂O₃ in NH₃, complete conversion of α -Ga₂O₃ to β -Ga₂O₃ was observed at \sim 780 °C.

Below 850 °C, the peak intensity of ZnO decreases with the increase of annealing temperature (see the lower panel of Figure 7) while the 2-theta angle shifts to lower values, indicating the thermal expansion of the ZnO. The decrease of the ZnO phase is also coincident with the formation of the spinel phase. The wurtzite structure of ZnO is maintained up to around 850 °C and no zinc nitride phase was detected. The ZnO phase is completely consumed when the intensity of the spinel phase reaches its peak. The wurtzite (Ga_{1-x}Zn_x)(N_{1-x}O_x) solid solution begins to form after the formation of the spinel intermediate phase. Once the spinel phase is consumed, the growth of the (Ga_{1-x}Zn_x)(N_{1-x}O_x) solid solution at 850 °C slows down, and the peak positions of the wurtzite phase shift to higher 2-theta and the peak widths become narrower with annealing time. Based on the lack of broad wurtzite GaN related XRD peaks and in consideration of its slow kinetics, formation of wurtzite GaN likely cannot compete with the formation of the solid solution. In the presence of excess ZnO (see Supporting Information, Figure S1, regarding the nitridation of a starting oxide mixture with Zn/Ga = 2:1), the nitridation and subsequent conversion of the spinel intermediate to the wurtzite phase takes less time. This indicates that the excess ZnO facilitates the reaction. Based on our in situ reaction studies, GaN does not enhance the reaction speed of the solid solution formation, even though the lattice constants of the solid solution are much closer to that of GaN than ZnO.

From the in situ XRD studies, it is clear that the formation of crystalline (Ga_{1-x}Zn_x)(N_{1-x}O_x) is related to the direct conversion of the spinel phase to wurtzite. Since the Zn/Ga ratio of spinel ZnGa₂O₄ is 0.5, the maximum bulk Zn/(Zn + Ga) ratio of the synthesized (Ga_{1-x}Zn_x)(N_{1-x}O_x) will be 1/3 regardless of the Zn/Ga ratio of the starting materials in the reaction.¹ The formation of the spinel phase is not dependent on the starting Ga₂O₃/ZnO ratio. When the Zn/Ga ratio in the starting material is less than 0.5, the stoichiometric excess of Ga₂O₃ is not incorporated into the ZnGa₂O₄ intermediate, but reacts with NH₃ to form GaN (see Supporting Information, Figure S2). In the case of Zn/Ga > 0.5, the excess ZnO is reduced to Zn by hydrogen from the pyrolysis of NH₃¹⁹ and then sublimates. According to a theoretical calculation on the correlation between the band gap and the composition of the (Ga_{1-x}Zn_x)(N_{1-x}O_x) solid solution,¹³ the smallest band gap energy should be obtained for a solid solution with composition of Zn/(Zn + Ga) \approx 0.5. To date, most photocatalysts prepared have had a Zn/(Ga + Zn) ratio below 1/3; the only exception reported in the literature is a value of 0.42 and corresponds to the smallest measured band gap for this material.⁴ To reach the smallest possible band gap in (Ga_{1-x}Zn_x)(N_{1-x}O_x) photocatalysts, the calculations suggest that other new synthesis approaches should be explored.

III.2. Stability and Structural Evolution of Wurtzite (Ga_{1-x}Zn_x)(N_{1-x}O_x): In Situ Time-Resolved XRD Studies. After the conversion of spinel ZnGa₂O₄ to wurtzite, the in situ XRD monitoring of the growth of the newly formed wurtzite phase revealed substantial structural changes during continued reaction with ammonia. The structural evolution of wurtzite (Ga_{1-x}Zn_x)(N_{1-x}O_x) involving the depletion of Zn and substitution of N by O can be better understood through systematic analysis of the XRD patterns of this stage. For this purpose, the in situ XRD patterns of the wurtzite phase were processed with Rietveld refinement to extract lattice constants, crystallite size, and atomic position information. In the refinement, GaN was used as a model even though the elemental content of the solid solution is unknown. Using GaN in place of (Ga_{1-x}Zn_x)(N_{1-x}O_x) as a model will still allow us to determine atomic positions,

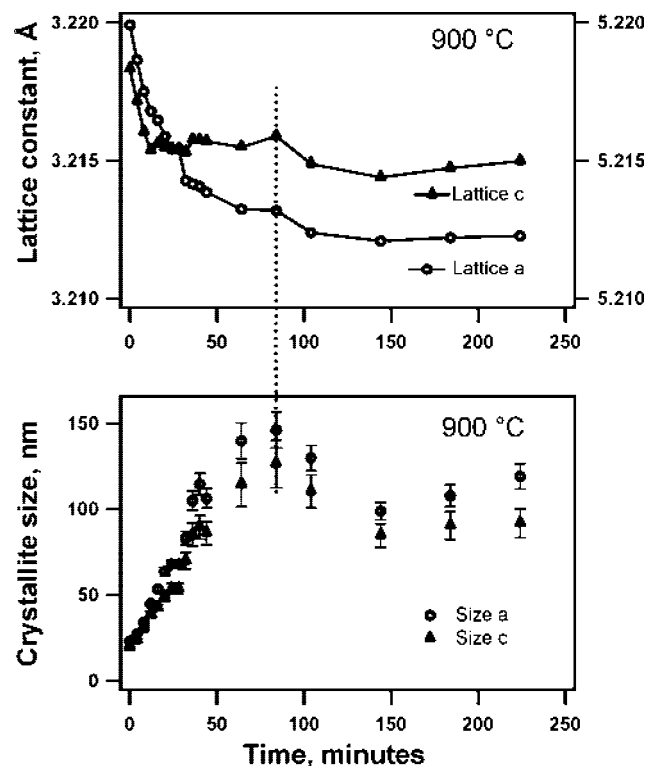


Figure 8. Rietveld refinement of the in situ XRD patterns of the wurtzite phase during the annealing of $\text{Ga}_2\text{O}_3/\text{ZnO}$ ($\text{Zn}/\text{Ga} = 1:1$) in an NH_3 atmosphere at $900\text{ }^\circ\text{C}$. In all figures, time zero is defined as the time when the wurtzite phase is formed by in situ XRD patterns. In this figure “a” denotes parameters along the symmetrically equal a - and b - axes, and “c” denotes those along the c -axis. In the middle panel, “lattice a” is associated with the left axis and “lattice c” with the right axis. The standard deviation for lattice constants is less than 0.001 \AA .

but not to distinguish between Ga and Zn, or N and O. Therefore for simplification, in the following discussion the Ga or Zn in the solid solution will be represented by M (metal) and the O and N by L (ligand). For a tetrahedrally coordinated metal atom, the metal–ligand bond along c -axis will be denoted as M_L_1 , and other bonds as M_L_3 . In the refinement of the atomic positions, only the fractional coordinate Z of the ligand at $(0.333333, 0.66667, Z)$ was refined. Refinement results at $900\text{ }^\circ\text{C}$ are presented in Figure 8 and Table 1.

As seen from Figure 8, the lattice constants of newly formed wurtzite phase decrease sharply, with the decrease of lattice a being larger than that of lattice c (0.2% vs 0.06%). After this rapid lattice-shrinking stage, the lattice constant c fluctuates within a narrow range while lattice a keeps decreasing. A slower lattice shrinkage process occurs simultaneously with the onset of crystallite size decrease.

From Table 1, it is clear that the ligand positions Z change with time. For the newly formed solid solution $Z = 0.382$, close to the 0.384 value of ZnO. The isotropic temperature factor $U_{\text{iso},L}$ is always larger than $U_{\text{iso},M}$, indicating larger thermal motion of the ligands. Overall, it appears that the ligands are “moving” along the c -axis during the structure evolution of wurtzite $(\text{Ga}_{1-x}\text{Zn}_x)(\text{N}_{1-x}\text{O}_x)$. Since the substitution of O by N is one of the main processes in the structure evolution, the substitution reaction may occur along the c -axis. Interestingly, for the newly formed wurtzite solid solution, its M_L_1 (1.993 \AA) is closer to ZnO (2.008 \AA) than to GaN (1.973 \AA). This observation may be used to account for the rate enhancement effect of ZnO on the nitridation reaction of both $\text{Ga}_2\text{O}_3/\text{ZnO}$ and ZnGa_2O_4 .

TABLE 1: Rietveld Refinement of Selected XRD Patterns of the Wurtzite Phase Formed during the Annealing of Ga_2O_3 and ZnO in NH_3 at $900\text{ }^\circ\text{C}$ ^a

time (min)	lattice a,b (\AA)	lattice c (\AA)	Z	M_L_1 (\AA)	M_L_3 (\AA)	$U_{\text{iso},M}$ (\AA^2)	$U_{\text{iso},L}$ (\AA^2)
ZnO	3.262	5.226	0.384	2.008	1.978	0.003*	0.018*
0	3.219	5.218	0.382	1.993	1.958	0.022	0.050
8	3.217	5.216	0.380	1.982	1.960	0.019	0.075
12	3.216	5.215	0.377	1.965	1.965	0.019	0.054
20	3.215	5.215	0.372	1.942	1.972	0.023	0.069
24	3.215	5.215	0.375	1.958	1.967	0.020	0.047
28	3.214	5.215	0.377	1.968	1.963	0.024	0.061
40	3.214	5.215	0.374	1.949	1.969	0.024	0.069
84	3.213	5.215	0.376	1.959	1.965	0.024	0.086
144	3.212	5.214	0.374	1.952	1.966	0.019	0.053
184	3.212	5.214	0.375	1.954	1.966	0.019	0.061
224	3.212	5.214	0.372	1.939	1.971	0.023	0.073
GaN	3.203	5.209	0.379	1.973	1.954	0.001*	0.053*

^a In the table, Z represents the fractional coordinates of the ligands in the unit cell of the wurtzite solid solution, and M_L_1 , M_L_3 are as depicted in Figure M2 of Supporting Information. $U_{\text{iso},M}$ and $U_{\text{iso},L}$ are isotropic temperature factors of metal and ligand. The lattice constants of GaN and ZnO in this table were converted to the lattice constant at $900\text{ }^\circ\text{C}$ using a thermal expansion coefficient of 1.0052 but the isotropic temperature factors are from room temperature data (denoted with an asterisk). The standard deviations for refined lattice constant, M_L_1 , M_L_3 are less than 0.001 \AA , 0.007 \AA , and 0.002 \AA , respectively.

TABLE 2: Ex Situ XRD and XAS of Wurtzite $(\text{Ga}_{1-x}\text{Zn}_x)(\text{N}_{1-x}\text{O}_x)$ Synthesized from the Annealing of $\text{Ga}_2\text{O}_3/\text{ZnO}$ in Ammonia at $850\text{ }^\circ\text{C}$ ^a

sample	Zn/Ga	lattice a,b (\AA)	lattice c (\AA)	M_L_1 (\AA)	M_L_3 (\AA)	M_{iso} (\AA^2)	L_{iso} (\AA^2)
ZnO		3.245	5.199	1.996	1.968	0.003	0.018
WZG_2h	0.22	3.199	5.193	2.032	1.931	0.008	0.013
WZG_10h	0.07	3.194	5.188	1.971	1.946	0.005	0.007
GaN		3.187	5.182	1.963	1.944	0.001	0.053

^a The Zn/Ga ratios were obtained from quantitative XANES analysis and the lattice constants were extracted using Rietveld powder refinement. The standard deviations for refined lattice constant, M_L_1 , M_L_3 are less than 0.001 \AA , 0.007 \AA , and 0.002 \AA , respectively.

III.3. Local Structure and Electronic Properties of $(\text{Ga}_{1-x}\text{Zn}_x)(\text{N}_{1-x}\text{O}_x)$: XAFS Studies. **III.3.1. Gallium and Zinc K-Edge XANES and EXAFS.** To examine the local structure of the solid solution, element-specific XAFS spectroscopic methods were employed. The discussion here is based on two samples, denoted WZG_2h and WZG_10h, prepared by annealing $\text{Ga}_2\text{O}_3/\text{ZnO}$ in ammonia at $850\text{ }^\circ\text{C}$ for 2 and 10 h, respectively, and then cooled to room temperature under an atmosphere of NH_3 . Both samples have wurtzite structure and their lattice constants were characterized by XRD and their Zn/Ga ratio determined by XANES (see Table 2). Sample WZG_2h, representative of newly formed $(\text{Ga}_{1-x}\text{Zn}_x)(\text{N}_{1-x}\text{O}_x)$, has a Zn/Ga ratio of 0.22 and is considered as the high-zinc content sample. Sample WZG_10h, with a Zn/Ga ratio of 0.07, is considered a low-zinc content sample. The structures are all at room temperature so it is easier to compare thermal parameters and make conclusions about disorder at ligand and metal sites. The thermal parameters of the metal are highest for the highest Zn content in the solid solution and much higher than the values observed for the pure GaN and ZnO. This is expected because high substitution of Zn in the solid solution would lead to high disorder at the metal site.

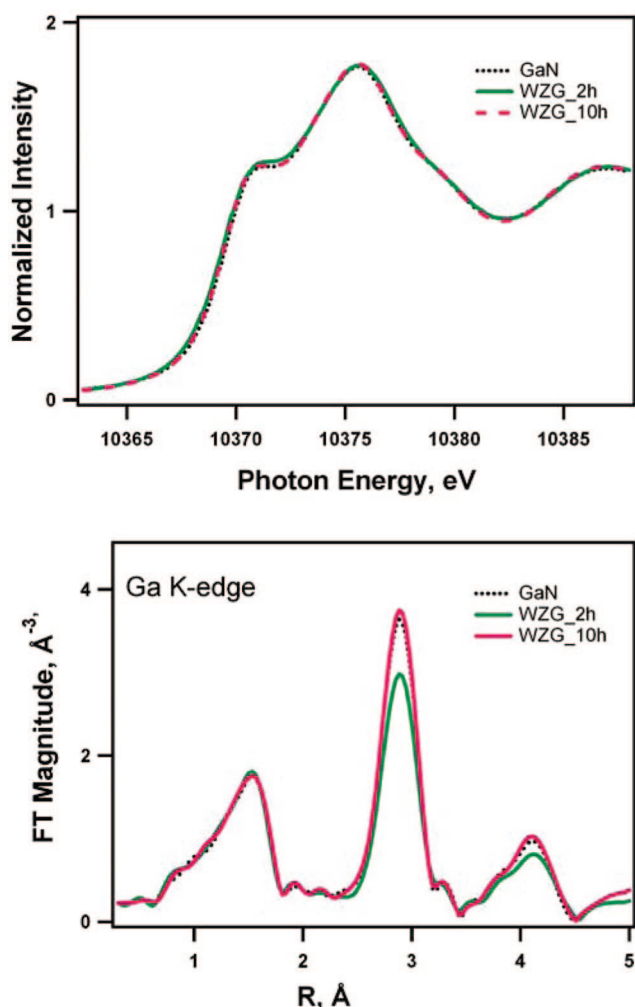


Figure 9. The XAFS (XANES and EXAFS) characterization of the Ga K-edge of the $(\text{Ga}_{1-x}\text{Zn}_x)(\text{N}_{1-x}\text{O}_x)$ samples and a GaN standard. Shown in the upper panel are the XANES spectra of the Ga K-edge. In the lower panel are nonphase-corrected Fourier transform (FT) magnitudes of the EXAFS spectra $\kappa^2\chi(\kappa)$ of the Ga K-edge.

Shown in the upper panel of Figure 9 are the XANES spectra of the Ga K-edge of GaN, WZG_2h, and WZG_10h. The XANES spectra of the two samples are the same as that of GaN, indicating that the local bonding geometry and oxidation state of Ga in the $(\text{Ga}_{1-x}\text{Zn}_x)(\text{N}_{1-x}\text{O}_x)$ are the same as they are in GaN. The EXAFS spectra are presented in the lower panel as Fourier transform magnitudes in R space. For GaN, the first shell of nearest neighbors (NN) consists of four nitrogen atoms and the second shell of NN contains 12 Ga atoms. In the lower panel of Figure 9, the peak near 1.6 Å corresponds to first-shell scattering and the peak near 2.9 Å corresponds to the combined second- and third-shell contributions.^{33,34} Compared to GaN, there are no peak position shifts or peak intensity variations associated with the feature at 1.6 Å for samples WZG_2h and WZG_10h, indicating the first shell of the two samples remain close to GaN regardless of their zinc content. For WZG_2h, the FT magnitude around 2.9 Å is reduced compared to that of GaN, suggesting a distortion of the second and third shell of Ga from standard GaN. No second and third shell distortion from GaN was observed for the low-zinc WZG_10h, indicating the distortion beyond the first shell is mainly due to the high zinc content in WZG_2h.

To obtain a more quantitative picture, theoretical fitting of the Ga K-edge EXAFS data was performed using FEFF6

theory³⁵ and Artemis data analysis package²⁴ to extract the interatomic distances. In the fitting, the GaN model and the theoretical coordination numbers are used in consideration of the large grain size. In the GaN model, the interatomic distances in each coordination shell fall into two groups with a bond length difference of $\sim 0.01\text{Å}$. In our calculations, only the average bond length of each coordination shell was used in the fit. The fitting results, including the interatomic distances and Debye–Waller factors, are tabulated in Table 3. As seen in Table 3, the interatomic distances and Debye–Waller factors of the first shell of both samples are close to those of GaN. For the second shell, the interatomic distances are close to GaN but the Debye–Waller factor of WZG-2 h is larger than that of GaN and the low-zinc WZG_10h as expected from visual examination of the data described above.

For the Zn K-edge, the XANES spectra (upper panel, Figure 10) show that the local bonding geometry of Zn in both samples is close to that of ZnO, but with the edge position red-shifted toward lower energies by $\sim 0.5\text{eV}$, indicating a lower oxidation state of Zn in $(\text{Ga}_{1-x}\text{Zn}_x)(\text{N}_{1-x}\text{O}_x)$ than in ZnO. Compared to ZnO, the peak positions associated with the first shell of WZG_2h and WZG_10h samples (lower panel of Figure 10) shift to longer NN distances and the FT magnitudes are reduced. There are also peak position shifts and FT magnitude reductions for the features associated with the second and third shells. Unlike Ga atoms, the distortion of short-range order of Zn atoms from ZnO in the $(\text{Ga}_{1-x}\text{Zn}_x)(\text{N}_{1-x}\text{O}_x)$ samples occurs in the first, the second, and/or third shell. We interpret this observation as follows: The lower the zinc content, the higher the distortion from ZnO; or the more dilute the zinc in $(\text{Ga}_{1-x}\text{Zn}_x)(\text{N}_{1-x}\text{O}_x)$, the more the chance for N to be at O sites and Ga at Zn sites, and the more difficult for Zn to keep its local chemical bonding close to that in ZnO.

The fitting of Zn K-edge EXAFS data (see Table 3) shows interatomic distance and Debye–Waller factor changes in all shells. Using ZnO as a standard, the first shell interatomic distances of both samples become longer as the zinc content becomes lower, while the second shell interatomic distances become shorter than those in ZnO. For the first two shells, the Debye–Waller factor increases with the decrease in zinc content in $(\text{Ga}_{1-x}\text{Zn}_x)(\text{N}_{1-x}\text{O}_x)$, suggesting higher disorder when zinc is dilute.

From bulk XRD data, the unit cell of the $(\text{Ga}_{1-x}\text{Zn}_x)(\text{N}_{1-x}\text{O}_x)$ solid solution is smaller than that of ZnO but close to that of GaN. If the Zn atoms can be perfectly confined at the Ga positions in GaN, then the Zn–ligand distance should be close to that in Ga–N. However, EXAFS data analysis showed that the first shell interatomic distance for Zn–O/N is longer than for Ga–N/O. In Table 2, the XRD data of wurtzite GaN, ZnO, and $(\text{Ga}_{1-x}\text{Zn}_x)(\text{N}_{1-x}\text{O}_x)$ solid solution shows that all the M_{L_1} is longer than M_{L_3} . It is therefore possible Zn–O/N bonds prefer to populate along the *c*-axis to accommodate longer Zn–O/N bonds in a GaN-dominant wurtzite lattice. This observation supports the theoretical calculations of Jensen et al.¹³ In the most stable hexagonal structure for the $(\text{Ga}_{12}\text{Zn}_4)(\text{N}_{12}\text{O}_4)$ supercell (see Figure 3c in their paper), the Zn–O bonds are preferably aligned along the *c*-axis.

III.3.2. Oxygen and Nitrogen K-Edge NEXAFS. The exploration of the local bonding geometry of N and O atoms on the $(\text{Ga}_{1-x}\text{Zn}_x)(\text{N}_{1-x}\text{O}_x)$ surface was carried out by NEXAFS, a characterization technique that probes the partial density of states (PDOS) in the conduction band of a semiconductor material. The features of the N K-edge NEXAFS spectrum represent the transition from an initial N

TABLE 3: Theoretical Fitting of Ga K-Edge and Zn K-Edge EXAFS Data Using FEFF⁶

$R, \text{\AA}$	>GaN	> $\sigma^2, \text{\AA}^2$	>WZG_2h	> $\sigma^2, \text{\AA}^2$	>WZG_10h	> $\sigma^2, \text{\AA}^2$
Ga K-Edge EXAFS Fitting						
1st Ga-N/O	1.940 (6)	0.0039 (6)	1.933 (4)	0.0033 (4)	1.936 (4)	0.0039 (4)
second Ga-Ga/Zn	3.189 (3)	0.0057 (3)	3.194 (3)	0.0071 (2)	3.190 (6)	0.0057 (10)
Zn K-Edge EXAFS Fitting						
1st Zn-O/N	1.963 (6)	0.0039 (5)	1.965 (5)	0.0052 (5)	1.975 (6)	0.0084 (8)
2nd Zn-Zn/Ga	3.230 (5)	0.0087 (3)	3.219 (5)	0.0099 (2)	3.208 (5)	0.0106 (3)

^a Tabulated are inter-atomic distances R and related Debye-Waller factors σ^2 up to three coordination shells. Wurtzite GaN was used as the model for the calculations and commercial GaN powder was used as a standard for Ga K-edge data fitting. For the Zn K-edge, wurtzite ZnO was used as the model for calculations and commercial ZnO powder was used as a standard.

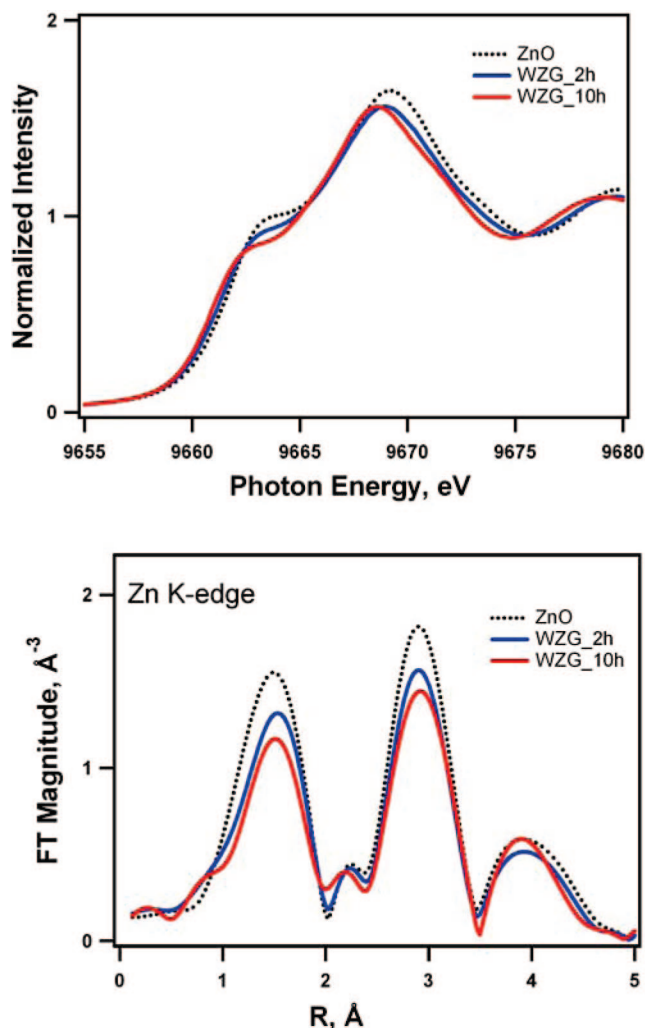


Figure 10. The XAFS (XANES and EXAFS) characterization of the Zn K-edge of the $(\text{Ga}_{1-x}\text{Zn}_x)(\text{N}_{1-x}\text{O}_x)$ samples and a ZnO standard. Shown in the upper panel are the XANES spectra of the Zn K-edge. In the lower panel are nonphase-corrected FT magnitudes of the EXAFS spectra $k^2\chi(k)$ of the Zn K-edge over a k range of 2.5 to 9 \AA^{-1} .

1s state to final states that contain contributions from p orbitals. Presented in the upper panel of Figure 11 are the nitrogen K-edge NEXAFS spectra of commercial GaN and two synthesized samples, WZG_sp and WZG_12h. Both samples were prepared by annealing $\text{Ga}_2\text{O}_3/\text{ZnO}$ in ammonia at a ramping rate of 2 to 850 $^\circ\text{C}$, holding the temperature at 850 $^\circ\text{C}$ for a certain amount of time, and then cooling to room temperature under an atmosphere of NH_3 . Sample WZG_sp was cooled down just after reaching 850 $^\circ\text{C}$ and sample WZG_12 was held at 850 $^\circ\text{C}$ for 12 h then cooled down in NH_3 atmosphere. Sample WZG_sp was a mixture

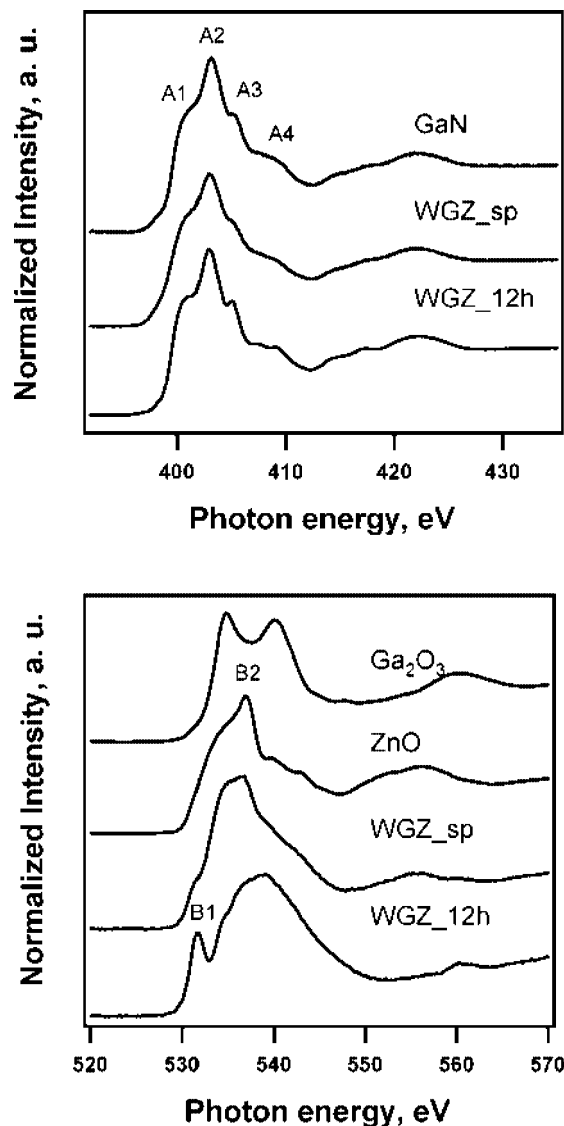


Figure 11. Surface sensitive NEXAFS spectra of the N K-edge and O K-edge of two synthesized samples, denoted WZG_sp and WZG_12h, and Ga_2O_3 , GaN, ZnO references. Both samples were prepared by annealing $\text{Ga}_2\text{O}_3/\text{ZnO}$ in ammonia as described in the text. Shown in the upper panel are nitrogen K-edge spectra and in the lower panel the oxygen K-edge spectra.

of spinel ZnGa_2O_4 and wurtzite $(\text{Ga}_{1-x}\text{Zn}_x)(\text{N}_{1-x}\text{O}_x)$. Sample WZG_12h was purely wurtzite $(\text{Ga}_{1-x}\text{Zn}_x)(\text{N}_{1-x}\text{O}_x)$. The GaN NEXAFS spectral features are similar to those reported in the literature.³⁶⁻³⁸ Peaks A1 to A3 correspond to 1s to $s + p_z$ transitions and peaks A2 and A4 correspond to 1s to $p_x + p_y$ transitions.³⁹ Compared to the NEXAFS spectrum of GaN, the spectrum of ZnGa_2O_4 -dominant sample WZG_sp displays

all the features that belong to GaN, but each feature is slightly broadened due to distortion. The similarity of the surface bonding environment of nitrogen atoms to that of GaN implies that the wurtzite $(\text{Ga}_{1-x}\text{Zn}_x)(\text{N}_{1-x}\text{O}_x)$ phase is on top of the dominant ZnGa_2O_4 spinel phase. The peaks of the WZG_12h NEXAFS spectrum are the same as those of GaN, but sharper. This means that the synthesized wurtzite $(\text{Ga}_{1-x}\text{Zn}_x)(\text{N}_{1-x}\text{O}_x)$ has better crystallinity than commercial GaN powder. Overall, the local bonding of nitrogen atoms in $(\text{Ga}_{1-x}\text{Zn}_x)(\text{N}_{1-x}\text{O}_x)$ is the same as that of GaN.

In contrast to nitrogen, the local bonding of oxygen atoms is not at all similar to that in ZnO. The oxygen K-edge NEXAFS spectra are displayed in the lower panel of Figure 11. For transition metal oxides, the O K-edge NEXAFS represents transitions from O 1s to unoccupied O 2p derived states from mixing of the O 2p with the Zn 4s,4p orbitals.⁴⁰ The NEXAFS spectral features of ZnO in Figure 11 are very similar to the features described in the literature^{40,41} and show an ideal stoichiometric ZnO with the prominent presence of the B2 feature ~ 537.0 eV. The B2 feature is greatly reduced in the spectrum of WZG_sp, and after the ZnGa_2O_4 in WZG_sp is completely converted to wurtzite (WZG_12h), the B2 feature is further reduced and a pre-edge feature B1 becomes prominent. The overall spectral features of the O K-edge of WZG_12h could not be attributed either to ZnO or Ga_2O_3 or to their linear combination. In an X-ray absorption study of As-doped ZnO, a similar pre-edge feature was observed and was believed to originate from holes at the O sites.⁴⁰ In consideration of the decreased oxidation state of Zn in the oxynitrides, assuming oxygen mainly bound to Zn, then the oxidation state of O will deviate from -2 . This slightly positive oxygen can be treated as the equivalent of a hole. On the other hand, if oxygen atoms occupy the nitrogen sites of the lattice, compared to the native N^{3-} , O^{2-} is deficient by one electron and could also be considered as a hole. A recent photoluminescence and photoluminescence excitation study of the optical properties of $(\text{Ga}_{1-x}\text{Zn}_x)(\text{N}_{1-x}\text{O}_x)$ suggested that visible light absorption occurs via Zn-related acceptor impurity levels.¹⁶ Formation of an impurity energy band from delocalized holes related to an acceptor or donor impurity are believed to be possible.¹⁶ This O K-edge NEXAFS pre-edge feature B2 associated with holes may be related to an impurity band that gives rise to the visible light activity of the $(\text{Ga}_{1-x}\text{Zn}_x)(\text{N}_{1-x}\text{O}_x)$ photocatalysts. However such an impurity band was not considered in the theoretical calculations of Jensen et al.¹³ that predicted the shrinking of the band gap to the visible-light portion of the spectrum.

IV. Conclusions

Gallium zinc oxynitrides are important compounds due to their visible-light photocatalytic activity.²⁻⁴ Our synchrotron based in situ reaction studies with time-resolved XRD and ex situ characterizations with XAFS have provided new insights into the mechanism for the synthesis of $(\text{Ga}_{1-x}\text{Zn}_x)(\text{N}_{1-x}\text{O}_x)$ compounds and their structural and electronic properties.

1. The spinel ZnGa_2O_4 was found to be a key intermediate in the production of $(\text{Ga}_{1-x}\text{Zn}_x)(\text{N}_{1-x}\text{O}_x)$ from the nitridation of ZnO/ Ga_2O_3 mixtures. The ZnGa_2O_4 intermediate and the instability of ZnO in NH_3 under reaction conditions impose a limit in the zinc content of the $(\text{Ga}_{1-x}\text{Zn}_x)(\text{N}_{1-x}\text{O}_x)$ systems. If ZnO/ Ga_2O_3 mixtures with a Zn/Ga ratio larger than $1/2$ are used, the excess ZnO is reduced to Zn by the hydrogen generated by the pyrolysis of NH_3 and then sublimates. In order to produce $(\text{Ga}_{1-x}\text{Zn}_x)(\text{N}_{1-x}\text{O}_x)$ compounds with an atomic zinc content higher than $1/3$, new synthesis approaches should be explored.

Furthermore, after its formation, the wurtzite $(\text{Ga}_{2/3}\text{Zn}_{1/3})(\text{N}_{2/3}\text{O}_{1/3})$ phase evolves to $(\text{Ga}_{0.9}\text{Zn}_{0.1})(\text{N}_{0.9}\text{O}_{0.1})$ with increasing nitridation reaction time as a result of the removal of Zn and O atoms from the system. Once $(\text{Ga}_{2/3}\text{Zn}_{1/3})(\text{N}_{2/3}\text{O}_{1/3})$ is formed, one must minimize exposure of this compound to NH_3 .

2. In the reaction of ZnGa_2O_4 with NH_3 , an elongation of the Zn–O bonds and compression of Ga–O bonds brings the interatomic distances into the range they exhibit in ZnO and GaN. The lengthening of the Zn–O bond could eventually lead to the break of the Zn–O bond and may be related to the depletion of Zn from the spinel ZnGa_2O_4 and $(\text{Ga}_{2/3}\text{Zn}_{1/3})(\text{N}_{2/3}\text{O}_{1/3})$. An apparent activation energy of 3.7 ± 0.3 eV was estimated for the ZnGa_2O_4 to $(\text{Ga}_{2/3}\text{Zn}_{1/3})(\text{N}_{2/3}\text{O}_{1/3})$ transformation. This value is close to the bond enthalpy of Ga–O, implying that Ga–O bond breaking may be the rate-limiting step in the formation of $(\text{Ga}_{1-x}\text{Zn}_x)(\text{N}_{1-x}\text{O}_x)$ from the reaction of ZnGa_2O_4 with ammonia.

3. XAFS data revealed that the local structures around gallium and zinc atoms in the $(\text{Ga}_{1-x}\text{Zn}_x)(\text{N}_{1-x}\text{O}_x)$ systems are similar to those of GaN and ZnO, respectively, with relatively minor distortions in the Ga–N and Zn–O bond lengths. As the zinc content decreases below $1/4$, the local bonding geometry and short-range order of the $(\text{Ga}_{1-x}\text{Zn}_x)(\text{N}_{1-x}\text{O}_x)$ deviates from that of ZnO and approaches that of GaN. The Zn–O/N bonds prefer to align along the *c*-axis of the lattice, in agreement with the findings of DFT calculations reported in the literature.¹³

4. The Zn K-edge XANES spectra of $(\text{Ga}_{1-x}\text{Zn}_x)(\text{N}_{1-x}\text{O}_x)$ display a position red-shifted toward lower energies by ~ 0.5 eV with respect to that of ZnO, indicating a lower oxidation state of Zn in $(\text{Ga}_{1-x}\text{Zn}_x)(\text{N}_{1-x}\text{O}_x)$. N K-edge NEXAFS data show that the bonding geometry and electronic properties of nitrogen atoms in $(\text{Ga}_{1-x}\text{Zn}_x)(\text{N}_{1-x}\text{O}_x)$ are similar to those in GaN. However, the O K-edge spectra exhibit a pre-edge feature not seen for ZnO or Ga_2O_3 . This unique property of the oxygen atoms in $(\text{Ga}_{1-x}\text{Zn}_x)(\text{N}_{1-x}\text{O}_x)$ may be related to the existence of holes and affect visible light absorption and surface chemistry.

Acknowledgment. The research carried out at the Chemistry Department of Brookhaven National Laboratory was funded by the U.S. Department of Energy, Division of Chemical Sciences (Contract Number: DE-AC02-98CH10086). This work is part of a DOE BES Hydrogen Fuel Initiative Project entitled “Catalyzed Water Oxidation by Solar Irradiation of Bang-Gap-Narrowed Semiconductors.” AIF and QW acknowledge support by U.S. DOE Grant No. DE-FG02-03ER15476. Beamlines X18B and X19A are supported in part by the Synchrotron Catalysis Consortium (U.S. DOE Grant No. DE-FG02-05ER15688). The NSLS is supported by the Divisions of Materials and Chemical Sciences of DOE. The authors would like to thank Dr. Nebojsa Marinkovic from the University of Delaware for help with the beamline operation.

Supporting Information Available: Figures of the ball-and-stick model, showing the structural changes from α - Ga_2O_3 to β - Ga_2O_3 , the XRD peak intensity variation with nitridation time, in situ XRD patterns during the annealing, and a comparison of the XRD patterns of the wurtzite phase and text discussing in situ XRD reaction studies of the nitridation. This material is available free of charge via the Internet at <http://pubs.acs.org>.

References and Notes

- (1) Ni, M.; Leung, M. K. H.; Leung, D. Y. C.; Sumathy, K. *Renew. Sustain. Energy Rev.* **2007**, *11*, 401.
- (2) Maeda, K.; Teramura, K.; Takata, T.; Hara, M.; Saito, N.; Toda, K.; Inoue, Y.; Kobayashi, H.; Domen, K. *J. Phys. Chem. B* **2005**, *109*, 20504.

- (3) Maeda, K.; Takata, T.; Hara, M.; Saito, N.; Inoue, Y.; Kobayashi, H.; Domen, K. *J. Am. Chem. Soc.* **2005**, *127*, 8286.
- (4) Maeda, K.; Teramura, K.; Lu, D. L.; Takata, T.; Saito, N.; Inoue, Y.; Domen, K. *Nature* **2006**, *440*, 295.
- (5) Maeda, K.; Teramura, K.; Lu, D. L.; Saito, N.; Inoue, Y.; Domen, K. *Angew. Chem., Int. Ed.* **2006**, *45*, 7806.
- (6) Maeda, K.; Teramura, K.; Lu, D. L.; Takata, T.; Saito, N.; Inoue, Y.; Domen, K. *J. Phys. Chem. B* **2006**, *110*, 13753.
- (7) Maeda, K.; Teramura, K.; Masuda, H.; Takata, T.; Saito, N.; Inoue, Y.; Domen, K. *J. Phys. Chem. B* **2006**, *110*, 13107.
- (8) Maeda, K.; Teramura, K.; Saito, N.; Inoue, Y.; Domen, K. *J. Catal.* **2006**, *243*, 303.
- (9) Maeda, K.; Teramura, K.; Saito, N.; Inoue, Y.; Kobayashi, H.; Domen, K. *Pure Appl. Chem.* **2006**, *78*, 2267.
- (10) Maeda, K.; Hashiguchi, H.; Masuda, H.; Abe, R.; Domen, K. *J. Phys. Chem. C* **2008**, *112*, 3447.
- (11) Maeda, K.; Teramura, K.; Domen, K. *Catal. Surv. Asia* **2007**, *11*, 145.
- (12) Maeda, K.; Teramura, K.; Lu, D. L.; Saito, N.; Inoue, Y.; Domen, K. *J. Phys. Chem. C* **2007**, *111*, 7554.
- (13) Jensen, L.; Muckerman, J. T.; Newton, M. D. *J. Phys. Chem. C* **2008**, *112*, 3439.
- (14) Yashima, M.; Maeda, K.; Teramura, K.; Takata, T.; Domen, K. *Chem. Phys. Lett.* **2005**, *416*, 225.
- (15) Yashima, M.; Maeda, K.; Teramura, K.; Takata, T.; Domen, K. *Mater. Trans.* **2006**, *47*, 295.
- (16) Hirai, T.; Maeda, K.; Yoshida, M.; Kubota, J.; Ikeda, S.; Matsumura, M.; Domen, K. *J. Phys. Chem. C* **2007**, *111*, 18853.
- (17) (a) Norby, P.; Hanson, J. C. *Catal. Today* **1998**, *39*, 301. (b) Wang, X.; Rodriguez, Hanson, J. C.; Gamarra, D.; Martinez-Arias, A.; Fernandez-Garcia, Marcos. *J. Phys. Chem. B* **2005**, *109*, 19595. (c) Rodriguez, J. A.; Hanson, J. C. *Ciencia* **2006**, *14*, 177.
- (18) Rehr, J. J.; Albers, R. C. *Rev. Mod. Phys.* **2000**, *72*, 621.
- (19) Chen, H. Y.; Nambu, A.; Wen, W.; Graciani, J.; Zhong, Z.; Hanson, J. C.; Fujita, E.; Rodriguez, J. A. *J. Phys. Chem. C* **2007**, *111*, 1366.
- (20) Chupas, P. J.; Chapman, K. W.; Kurtz, C.; Hanson, J. C.; Lee, P. L.; Grey, C. P. *J. Appl. Crystallogr.* **2008**, *41*, 822.
- (21) Chupas, P. J.; Ciruolo, M. F.; Hanson, J. C.; Grey, C. P. *J. Am. Chem. Soc.* **2001**, *123*, 1694.
- (22) Toby, B. H. *J. Appl. Crystallogr.* **2001**, *34*, 210.
- (23) Sambasivan, S.; Fischer, D. A.; Shen, M. C.; Hsu, S. M. *J. Biomed. Mater. Res., Part B* **2004**, *70B*, 278.
- (24) Ravel, B.; Newville, M. J. *Synchrotron Radiat.* **2005**, *12*, 537.
- (25) Tas, A. C.; Majewski, P. J.; Aldinger, F. *J. Am. Ceram. Soc.* **2002**, *85*, 1421.
- (26) Jung, W. S. *Mater. Lett.* **2002**, *57*, 110.
- (27) Jung, W. S. *Mater. Lett.* **2006**, *60*, 2954.
- (28) Phani, A. R.; Santucci, S.; Di Nardo, S.; Lozzi, L.; Passacantando, M.; Picozzi, P.; Cantalini, C. *J. Mater. Sci.* **1998**, *33*, 3969.
- (29) *CRC Handbook of Chemistry and Physics*, 72nd ed.; CRC Press: Boca Raton, FL, 1992.
- (30) Norby, P.; Christensen, A. N.; Hanson, J. C. *Inorg. Chem.* **1999**, *38*, 1216.
- (31) Norby, P. *J. Am. Chem. Soc.* **1997**, *119*, 5215.
- (32) Chupas, P. J.; Chapman, K. W.; Jennings, G.; Lee, P. L.; Grey, C. P. *J. Am. Chem. Soc.* **2007**, *129*, 13822.
- (33) Yu, K. M.; Shan, W.; Glover, C. J.; Ridgway, M. C.; Wong, W. S.; Yang, W. *Appl. Phys. Lett.* **1999**, *75*, 4097.
- (34) Miyano, K. E.; Woicik, J. C.; Robins, L. H.; Bouldin, C. E.; Wickenden, D. K. *Appl. Phys. Lett.* **1997**, *70*, 2108.
- (35) Zabinsky, S. I.; Rehr, J. J.; Ankudinov, A.; Albers, R. C.; Eller, M. J. *Phys. Rev. B* **1995**, *52*, 2995.
- (36) Hecht, J. D.; Frost, F.; Hirsch, D.; Neumann, H.; Schindler, A.; Preobrajenski, A. B.; Chasse, T. *J. Appl. Phys.* **2001**, *90*, 6066.
- (37) Katsikini, M.; Paloura, E. C.; Antonopoulos, J.; Bressler, P.; Moustakas, T. D. *J. Cryst. Growth* **2001**, *230*, 405.
- (38) Petravic, M.; Deenapanray, P. N. K.; Coleman, V. A.; Kim, K. J.; Kim, B.; Li, G. *J. Appl. Phys.* **2004**, *95*, 5487.
- (39) Lawniczak-Jablonska, K.; Suski, T.; Gorczyca, I.; Christensen, N. E.; Attenkofer, K. E.; Perera, R. C. C.; Gullikson, E. M.; Underwood, J. H.; Ederer, D. L.; Weber, Z. L. *Phys. Rev. B* **2000**, *61*, 16623.
- (40) Vaithianathan, V.; Lee, B. T.; Chang, C. H.; Asokan, K.; Kim, S. S. *Appl. Phys. Lett.* **2006**, *88*.
- (41) Ray, S. C.; Low, Y.; Tsai, H. M.; Pao, C. W.; Chiou, J. W.; Yang, S. C.; Chien, F. Z.; Pong, W. F.; Tsai, M. H.; Lin, K. F.; Cheng, H. M.; Hsieh, W. F.; Lee, J. F. *Appl. Phys. Lett.* **2007**, *91*.